SOLUTION MINING RESEARCH INSTITUTE
www.solutionmining.org

105 Apple Valley Circle
Clarks Summit, PA 18411, USA

Telephone: +1 570-585-8092

Technical Conference Paper

In-situ Permeability Test in a Salt Formation at Marboz, France

Sivaprasath Manivannan
LMS, Ecole Polytechnique, Palaiseau, France

Jean Barottin
INOVYN, Tavaux, France

Pierre Bérest
LMS, Ecole Polytechnique, Palaiseau, France

Benoît Brouard
Brouard Consulting, Paris, France

Vincent de Greef
LMS, Ecole Polytechnique, Palaiseau, France

Antoine Jacques[4]
TOTAL SA, Pau, France

SMRI Fall 2018 Conference
24-25 September 2018
Belfast, Northern Ireland, UK

In-situ Permeability Test in a Salt Formation at Marboz, France

Sivaprasath Manivannan[1], Jean Barottin[2], Pierre Bérest[1], Benoît Brouard[3], Vincent de Greef[1], Antoine Jacques[4]

[1]LMS, Ecole Polytechnique, Palaiseau, France
[2]INOVYN, Tavaux, France
[3] Brouard Consulting, Paris, France
[4]TOTAL SA, Pau, France

Abstract

Permeability tests were performed in a 1698-m deep wellbore drilled from the Bresse salt formation at Marboz. During Phase 1, the wellbore was filled with brine, and the wellhead pressure was increased to 18 bars (260 psi) and 37 bars (536 psi), successively. Pressure evolution was recorded over 19 days and 28 days, respectively. It is governed by creep closure and permeation through the open hole, the casing shoe and the steel casing. Back-calculations prove that wellbore permeability is around 6×10^{-21} m^2. During Phase 2, diesel was injected to develop a brine-diesel interface in the external annulus, and wellhead pressure was kept constant using a pressure regulator. Diesel permeation to the rock formation can be considered negligible; permeation is through the open hole. The interface first was set below the casing shoe over a 17-day period, then at three deeper locations in the open hole for shorter periods. This procedure allows assessing the average permeability of various parts of the well. The average permeability of the open hole proved to be 4×10^{-21} m^2, a very low value. The testing method was not accurate enough to allow estimation of the average permeability of smaller intervals in the open hole. Longer testing periods and more accurate pressure sensors might allow such an estimation.

1 Introduction

INOVYN operates a brine field at Marboz in the *département* of Ain, France. In the same Bresse salt formation, about 10 km (6 miles) from this brine field, twenty gas-storage caverns are operated by the utility company Storengy. The salt formation includes two thick layers separated by a "sterile" intermediate layer whose insoluble content is high. At Étrez, the lower salt layer (having top and bottom with depths of 1340-m (4396 ft) and 1970-m (6463 ft) deep, typically) contains fewer impurities (Curial, 1986) and is considered generally to be less permeable than the upper layer.

In 2017, a borehole (AT032) was drilled at Marboz. It remained available for testing for a couple of months before solution mining began. It was decided to perform a multi-step test to assess the permeability of the salt formation. Brouard et al. (2001) had reviewed a dozen of Mechanical Integrity Tests performed at Étrez. During these tests, a packer was set a few meters above the casing shoe (to isolate any leak through the casing), and water was injected into the tubing twice a day to

maintain a constant testing gradient. The average permeability of the "lower salt layer + casing shoe" estimated from these tests was in the 4.6 – 19 x 10^{-21} m² range.

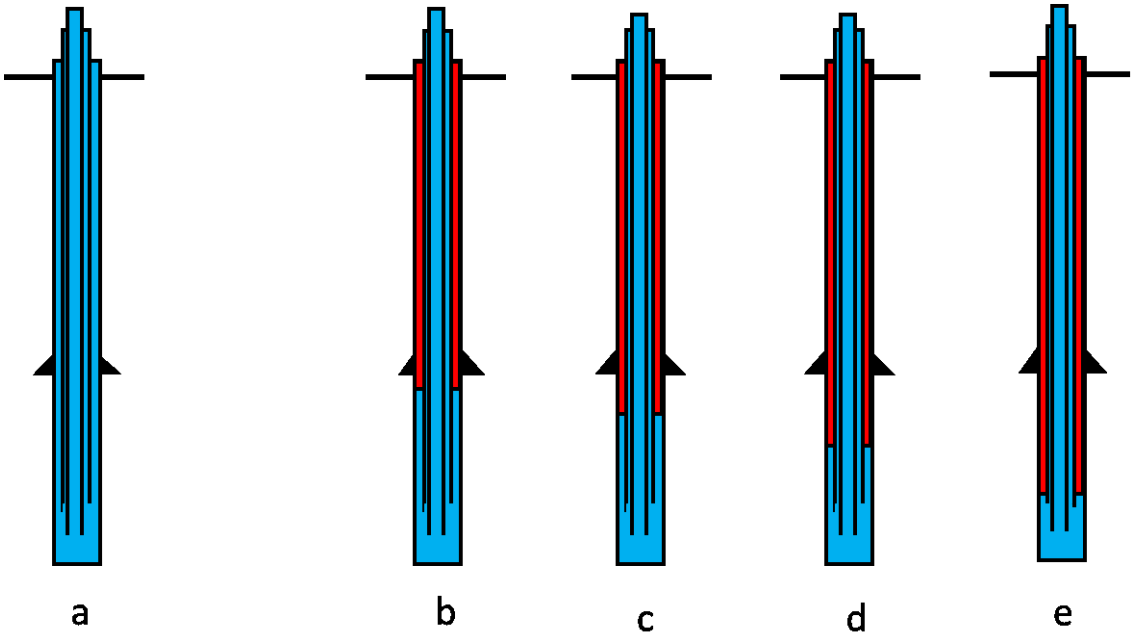

Figure 1: Brine permeability test (a) and "MIT" test (b), an attempt to test formation permeability as a function of depth (b, c, d)

The test at Marboz was two-fold (see Fig.1). During the first phase (Fig. 1a), the wellbore was filled with brine, and wellhead pressure was increased to 18 bars (260 psi) and 37 bars (536 psi), successively. After each pressure increase, wellhead pressure evolution was measured over 19 days and 28 days, respectively. The average permeability of the well was estimated from these pressure evolutions; it includes brine seepage through the open-hole walls, and leaks through the casing shoe and the steel casing.

The second phase was an attempt to measure the permeability of the open hole as a function of depth: diesel was injected in the annular space to develop a brine-diesel interface at various depths. (Rock salt is considered to be almost impermeable to diesel, due to capillary pressure and the low relative permeability of brine-saturated salt.) At the beginning of the second phase, the interface was lowered a few meters below the casing shoe (Fig 1b), and wellhead pressure was maintained constant through brine injection into the central string. Permeability of the open hole alone was estimated from the wellhead injection rates. Then, the interface was lowered to three greater depths (Figs. 1c, 1d, 1e), and injection rates were measured in an attempt to differentiate between the permeabilities of various parts of the open hole. However, this permeability was so small that the designed method was not accurate enough to differentiate the permeability variations (if any) in

the open hole. This method, whose objective is to assess permeability as a function of depth in a borehole, is called "*discrete WTLog*" (Manivannan et al., 2017).

2 Well geometry

The well is 1698-m (5571 ft) deep and 1747-m (5732 ft) long, with a deviated section in the lower part of the cemented well (Fig. 2). The diameter of the last cemented casing is $11^{3/4}$". The casing shoe is set at 1346 m (4416 ft) true vertical depth (TVD). The open hole has a vertical section 352 m (1155 ft) long and runs entirely through the lower salt layer. Two strings, with diameters $5^{1/2}$" and $8^{5/8}$", respectively, were run in the wellbore, creating three different spaces in the upper part of the well: a central string, an intermediate annulus, and an external annulus. Lengths — i.e., measured depth (MD) — and internal volumes of these three spaces are given in Table. 1.

The overall volume of the open hole, as measured by caliper log, is 51.72 m^3, (1826 ft^3) which is 2.2 m^3 (78 ft^3) larger than the volume computed using nominal cross-sectional areas. It is highly likely that the cross- section of the open hole is not uniform. The computed volume of the fluid contained in the $8^{5/8}$" x $11^{3/4}$" external annulus, above the casing shoe, is 29.42 m^3 (1039 ft^3).

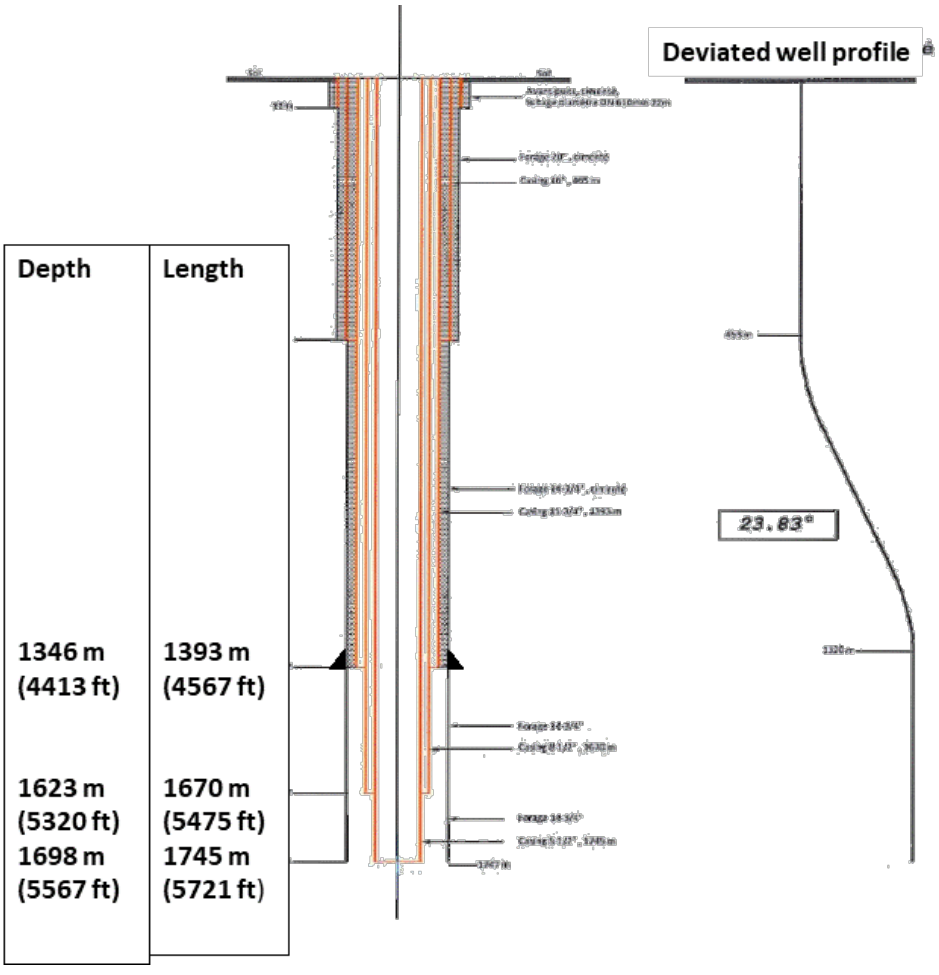

Figure 2: Schematic of the well.

Table 1: AT032 cross-sections (*nominal value — the as-measured value is slightly larger).

	Length m (MD)	External diameter (mm)	Internal diameter (mm)	Cross-sectional area (L/m)
$5^{1/2}$"	1745	139.70	121.30	11.56
$8^{5/8}$"	1670	219.08	201.28	16.49 ($5^{1/2}$" x $8^{5/8}$")
$11^{3/4}$"	1393	298.45	273.65	21.12 ($8^{5/8}$" x $11^{3/4}$")
Open hole	1747-1393	374.65		72.55* ($8^{5/8}$" x $14^{3/4}$") 94.91* ($5^{1/2}$" x $14^{3/4}$")

3 Rock and fluid properties

The temperature measured at 1698 m (TVD) is 65 °C. The overburden pressure gradient is approximately γ_R = 0.22 bar/m (1 psi/ft). Figure 3 shows the density and the viscosity of the fluids used in the test as a function of temperature. The hydro-static pressure gradient of the brine column, computed using the brine density at 20 °C, is γ_b = 0.116 bar/m (0.513 psi/ft).

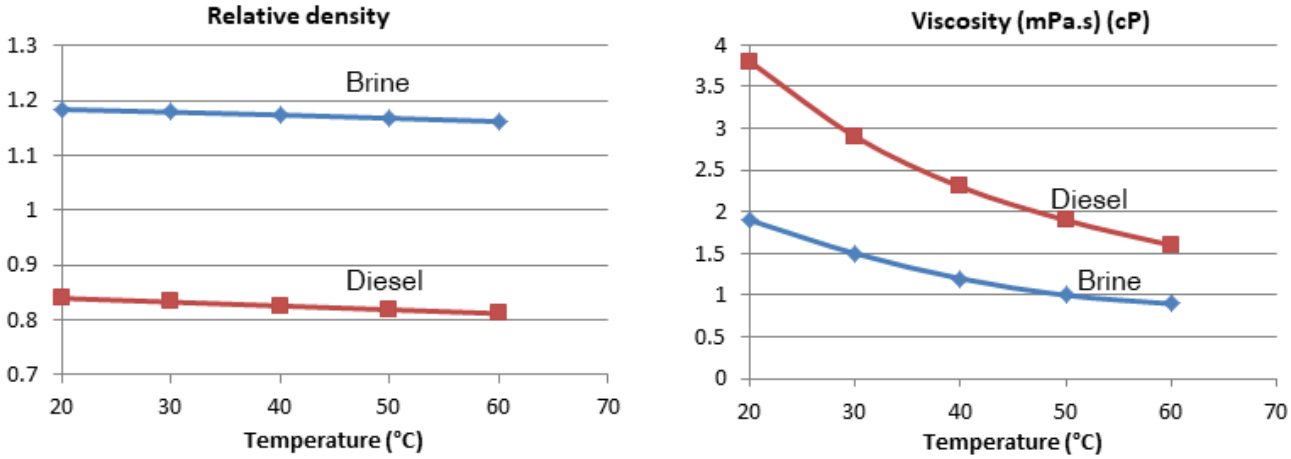

Figure 3: Relative density and viscosity of the brine and the diesel used during the test.

4 Test procedure and equipment

4.1 Phase 1

On February 14, 2018, the wellhead-tubing pressure was increased from 0 to 18 bars (261 psi) by injecting brine in the central tubing. By dividing the injected brine volume, δV, by the wellhead pressure change, δP, well compressibility was estimated to be δV / δP = βV = 3.8 L/bar (0.07 gallon/psi). The well was kept closed, and the pressure evolution was recorded by a pressure sensor at the central tubing wellhead over 19 days, from February 14 to March 5 (Fig. 4, left). The well was depressurized for a workover that lasted one week. On March 12, the well was re-

pressurized to 37 bars (537 psi), and evolution of the tubing wellhead pressure was measured for 28 days (until April 10).

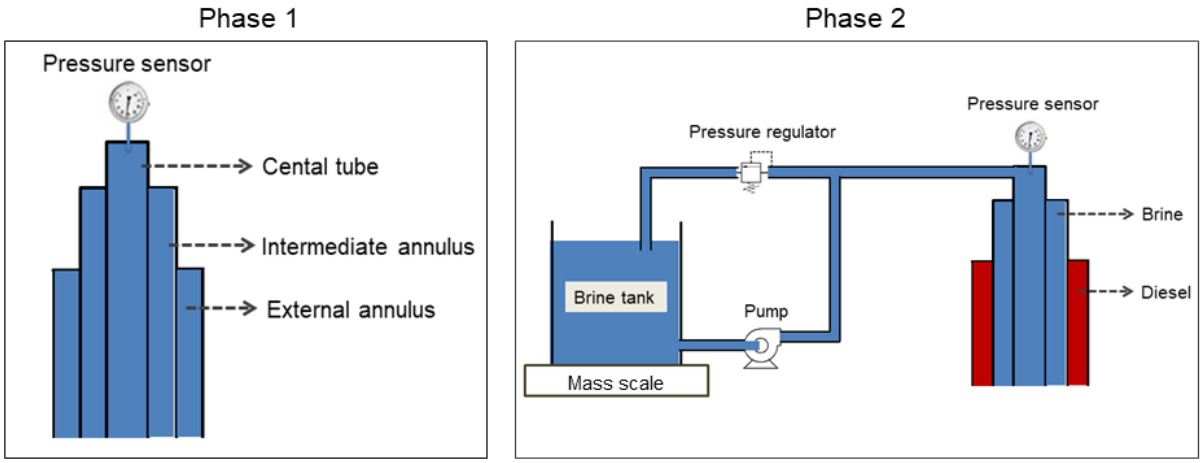

Figure 4. Wellhead schematic design: (left) during Phase 1; left, when the well is shut-in); and (right) during phase 2, pressure regulation system injects brine into the tubing to maintain constant wellhead pressure.

Table 2: Test schedule during Phase 1 (effecting a change in wellhead pressure).

Date	Wellhead pressure	Duration (days)	Comments
February 14, 2018	18 bars (261 psi)	19	First pressure step of Phase 1
March 5, 2018	0 bar	7	Workover
March 12, 2018	37 bars (537 psi)	28	Second pressure step of Phase 1

4.2 Phase 2

On April 11-12, 30 m^3 (190 bbls) of diesel were injected (over 2 days) in the external annulus, and a similar volume of brine was removed from the central tubing. This placed the brine-diesel interface just below the casing shoe. At the end of this injection, wellhead pressure was 39 bars (565 psi) at 3 pm on April 12. A pressure regulation system was added to maintain constant pressure at the tubing wellhead. A schematic of the pressure regulation system is shown in Fig. 4 (right). When the well-head pressure is less than the desired value, the choke in the pressure regulator remains closed. When the pressure is higher, the choke opens, brine is withdrawn from the tubing, and the prescribed pressure is re-established. A scale measures the mass of the brine contained in the storage tank with an accuracy of 0.05 kg. As before, the tubing wellhead pressure was measured by a pressure sensor. Note that after the April 11-12 injection, the pressure drop was so swift that it could not be accommodated fully by the regulation system, whose maximum injection rate is 14 L/day (3.5 gallon/day). It took nearly 6 days for the pressure to be reestablished at about 43 bars.

After April 30, the brine-diesel interface was lowered to greater depths through additional diesel injections, and the test was repeated. These tests were shorter than the earlier ones, lasting 4-10 days each (Table 3); their objective was to estimate possible heterogeneities in the permeability of the open hole.

Table 3: Test schedule during Phase 2 (diesel injections). [The tested length from 1393 m (4567 ft) to 1670 m (5470 ft).]

Date	Diesel volume injected (m^3)	Interface location	Test duration (days)
April 11-12	30	Just below the casing shoe	17
April 20	6.7	1/3rd of the tested length	9
May 9	6.77	2/3rd of the tested length	5
May 14	6.7	Bottom of the 8$^{5/8}$" tube	4

Figure 5 shows the tubing wellhead pressure recorded daily at 18h00 (6 pm) during the entire test. The wellhead brine-injection rate (in the tubing) during Phase 2 is shown in Fig. 6. The brine injection rates are computed by dividing the daily change in the mass of the tank brine by brine density (1184 kg/m^3).

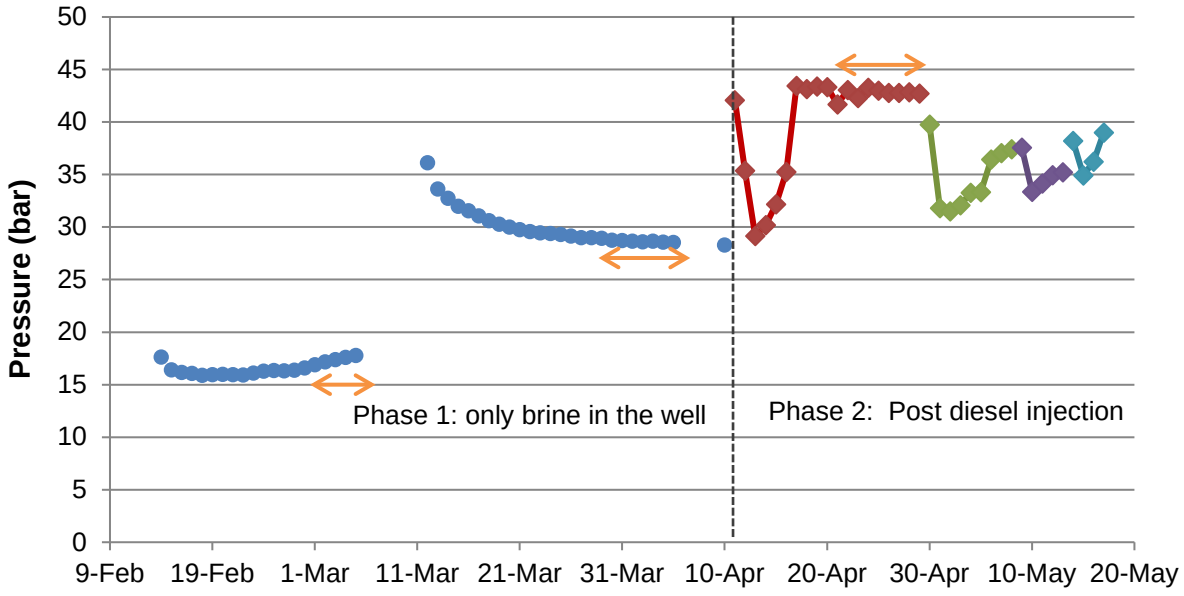

Figure 5: Tubing wellhead pressure (measured daily at 6 pm) during the duration of the entire test.

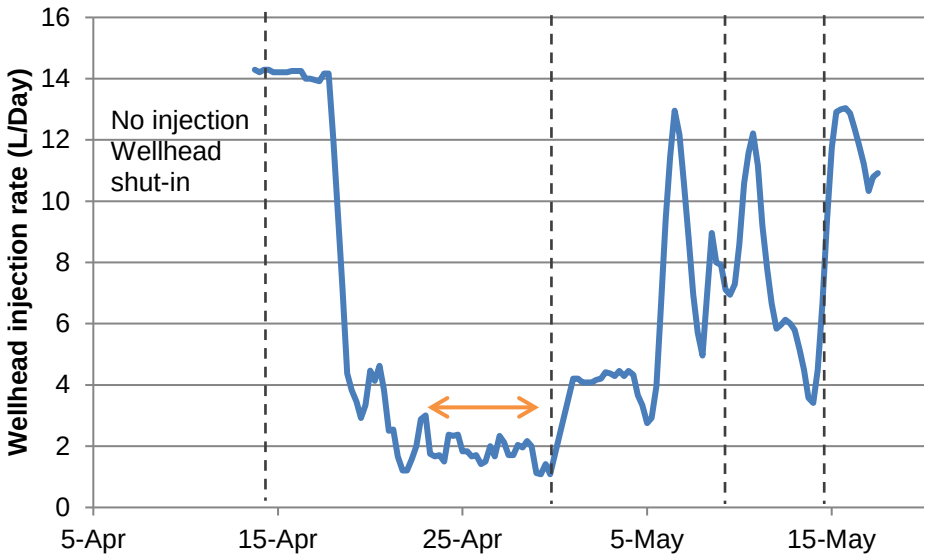

Figure 6: Wellhead brine-injection rate during Phase 2.

5 Physical phenomena

After a swift fluid injection (or withdrawal), pressure evolution in a shut-in wellbore is governed by several effects, including temperature changes, additional salt dissolution, creep closure and brine permeation through the cavern walls.

Thermal effects and additional dissolution are early time effects; they are effective mostly during a short period (1 - 4 days) after a thermal or chemical disequilibrium is created. Creep closure and brine permeation are much slower processes.

5.1. Thermal effects occur when the wellbore fluid temperature is different from the geothermal temperature of the rock mass. Liquids warming or cooling in the wellbore leads to changes in fluid volumes and densities, resulting in pressure changes in a shut-in well (Skaug et al., 2011; Lampe and Ratigan, 2014; Manivannan et al., 2015).

Consider first the effects of daily (night/day) temperature changes at ground level. In the upper part of the wellbore, at shallow depths (typically, less than a dozen meters), liquid temperature is the sum of average temperature and daily fluctuations, $\boldsymbol{T}(\boldsymbol{r},\boldsymbol{t}) = \boldsymbol{T}_{\boldsymbol{av}}(\boldsymbol{z}) + \theta(\boldsymbol{z},\boldsymbol{t})$. These fluctuations can be integrated with respect to depth along the wellbore. (For simplicity, no string is taken into account):

$$I(t) = \int_0^H \theta(z,t)dz$$

where H is the borehole depth (From a practical perspective, daily fluctuations are exceedingly small when z > 10 m, see Brouard et al., 2013.)

These temperature changes lead to a liquid volume change by $\alpha SI(t)$, where S is the wellbore cross-sectional area (S = 60 L/m is typical.); $I(t)$ as defined above; α is the liquid thermal expansion coefficient (For brine, α = 4.4 10^{-4}/°C; for diesel, α = 10^{-3}/°C are typical.), and to a cavern pressure change by $\alpha SI(t) / \beta V$, where βV is the compressibility of the wellbore. (At Marboz, βV = 3.8 L/bar when the wellbore is filled with brine.) In addition, as the liquid density in the wellbore changes, the difference between wellbore average pressure and wellhead pressure increases by $\rho g\, \alpha I(t)$. The overall wellhead pressure change is

$$(S / \beta V + \rho g)\, \alpha I(t)$$

The value $S/\beta V$ = 1.5 x 10^6 Pa/m is much larger than ρg = 1.2 x 10^4 Pa/m (The opposite is true in a full-size cavern.), and the pressure change is $S\alpha /\beta V$ = 660 Pa/°C-m. The maximum possible value of $I(t)$ must be computed (or measured) on a case-by-case basis. During the initial days of Phase 1, the daily fluctuations in ambient temperature were quite small due to the winter weather. Assuming that the temperature fluctuations in the wellbore are uniform (≈3 °C) and limited to 10 m below the wellhead, the amplitude of $I(t)$ can be given as 30 °C-m. This translates into daily pressure fluctuations of 0.2 bars (3 psi), not far from the magnitude of the fluctuations observed in Fig. 7. During Phase 2, the wellbore contains diesel oil, which has a relatively large thermal expansion coefficient; also, $I(t)$ can be as large as several dozens of °C-m due to larger temperatures fluctuations in the spring.

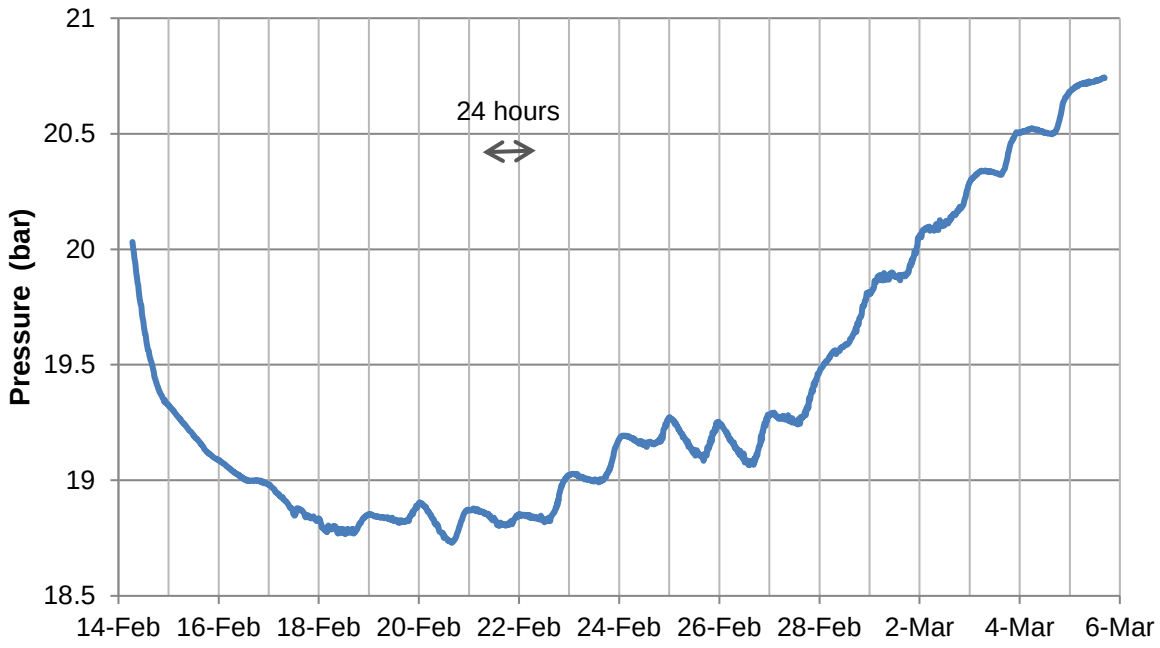

Figure 7: Tubing wellhead pressure during Phase 1. [The small fluctuations in wellhead pressure (with a time period of 24 hours) is due to daily fluctutations in ambient temperature.

Consider, now, the effects of cold diesel injection during Phase 2. On April 11-12, 30 m^3 of cold diesel were injected in the external annulus; the brine contained in the central string (20 m^3) was withdrawn together with 10 m^3 of hot brine (65 °C) contained in the lower part of the borehole. As a result, the central string was filled with hot brine. Straightforward computations proved that, as a whole, wellbore liquids cooled after injection was completed, leading to a large pressure drop from April 11 to 13 (Fig. 5). Such an effect did not exist during Phase 1, as no brine was withdrawn from the central tubing.

5.2. Additional dissolution/re-crystallization of salt occurs because the concentration of brine at saturation is an increasing function of pressure (and temperature). When brine pressure increases, additional dissolution takes place, leaving more space for brine and reducing the magnitude of the original pressure change. This process ends after the brine is saturated in the new pressure conditions (Bérest et al., 2007).

When these two transient effects vanish, long-term creep closure and permeation can be observed.

5.3. ***Long-term creep closure*** of the open hole occurs due to the visco-plastic behavior of salt. Wellbore pressure in the open hole typically is smaller than the overburden pressure, leading to creep closure and a gradual reduction in the open-hole volume. When the wellhead is closed, the reduction in the open-hole volume manifests itself as pressure increase. The long-term creep closure rate decreases when wellhead pressure increases.

5.4. Permeation of the wellbore fluid into the salt/rock formation. Pore pressure in the salt formation is difficult to assess. In the Bresse salt formation, Durup (1994) proved that it was close to halmostatic pressure ($P_h = \gamma_b z$) and that permeation obeys Darcy law. When the well is filled with brine with pressure higher than halmostatic, brine permeation occurs, fluid mass in the wellbore decreases, and brine pressure drops.

These two last phenomena have opposite effects: (1) creep closure rate decreases when brine pressure increases and vanishes when brine pressure is geostatic ($P_\infty = \gamma_R z$); and (2) permeation rate vanishes when brine pressure is halmostatic ($P_h = \gamma_b z$) and increases when brine pressure increases. In principle, brine pressure remains constant when the creep-closure rate exactly equals the permeation rate.

6 Results

In Fig. 5 (repeated for convenience), after the wellbore pressure was increased to 18 bars (261 psi) on February 14, a transient pressure decrease was observed. After 3 - 4 days, wellhead pressure stabilized, then increased, suggesting that when wellhead pressure is 18 bars or less, the brine-permeation rate is smaller than the creep-closure rate. After 19 days (since the beginning of the test), the well was kept open for one week. On March 12, the wellhead pressure was increased to 37 bars (537 psi). The transient pressure decrease was steeper than when the initial pressure increase was 18 bars; the pressure kept decreasing, suggesting that, when wellhead pressure is larger than 37 bars, the permeation rate is faster than creep closure rate. The wellhead pressure at the end of Phase 1 was 28.3 bars (410 psi). It is likely that an equilibrium wellhead pressure should be reached, somewhere between 20 bars (290 psi) and 28.3 bars (410 psi), such that permeation equals creep rate and the wellhead pressure remains constant. However, the test duration is too short to draw definite conclusions.

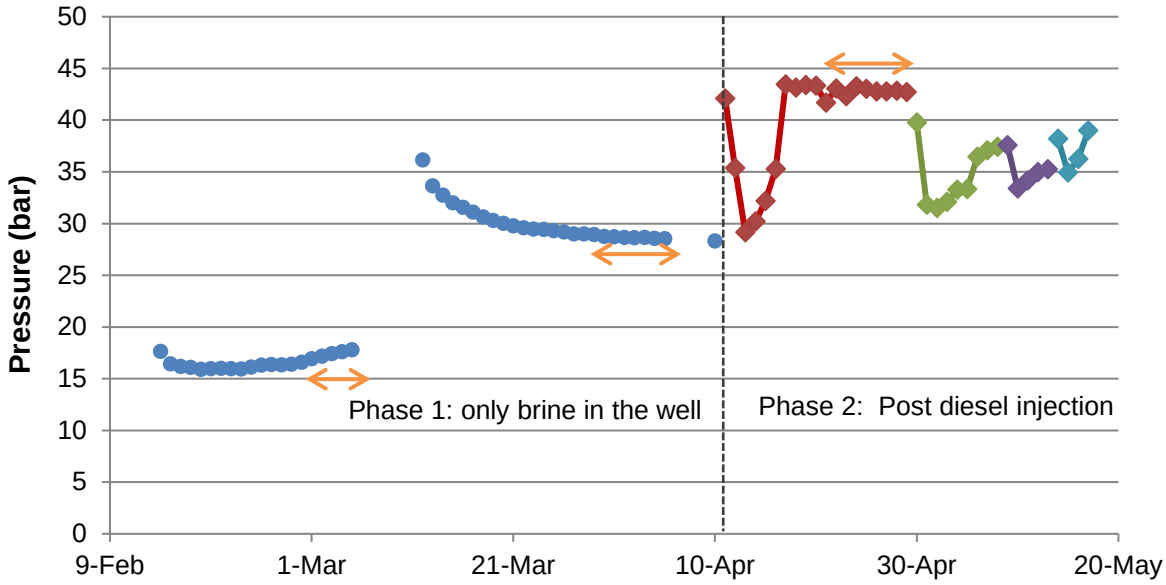

Figure 5 (repeated): Tubing wellhead pressure (measured at 6 pm daily) during the entire test duration.

During the initial days of Phase 2, the pump injection rate was at its maximum power (14 L/day, or 4 gallons /day); however, it was not able to restore the initial pressure, as thermal effects were too large. It is only after 5 - 6 days, after these effects vanish, that the regulation system was able to increase the wellhead pressure to 43 bars (Figs. 5 and 7). The additional salt-dissolution effects persist for another 3 - 4 days. After April 24, the injection rate at wellhead approximately equaled the permeation rate minus the creep-closure rate; it is about 1.8 L/day (half a gallon per day). When the interface was lowered further on April 30, the cycle repeated. However, this time, the pump does not seem to be injecting at its maximum power. Some salt crystallization was observed in the pump at the end of the test. Data after April 30 are not interpretable, as there was no pressure

stabilization. (Test duration was too short, due to operational constraints; in addition, open-hole permeability was so small that differentiating the permeabilities of the different parts of the open hole was impossible).

7 Interpretation

When pressure changes are small, the short time transients, such as additional dissolution and temperature changes, become negligible after a few days. This is the case during the periods marked on Fig. 5 by orange double-headed arrows, which will be used, below, for quantitative interpretation.

7.1 Creep closure in the open hole

Creep closure raises a difficult problem. To describe steady-state creep, a Norton Hoff creep law ($d\varepsilon/dt = A^*(T)\ \sigma^n$) often is accepted; simple calculations prove that, for a cylindrical hole, the resulting steady-state creep closure rate can be written as

$$dV/dt = C_{creep}^{ss}(T,n)\ \Delta P^n \tag{1}$$

where ΔP is the gap between geostatic pressure and borehole pressure, and $C_{creep}^{ss}(T,n) = \sqrt{3}\ \left(\frac{\sqrt{3}}{n}\right)^n /2$. However, numerical computations prove that, in a wellbore, transient creep is much longer (many years) than in the case of a test on a cylindrical sample (several months), because of slow stress redistribution (Manivannan and Bérest, 2018). To allow simple computations, it is accepted that Eq. (1) still holds and that exponent n is identical to the exponent that describes the results of tests performed on salt samples. The steady-state creep coefficient, C_{creep}^{ss}, is replaced by a pseudo steady-state coefficient C_{creep}, which remains constant during the relatively brief test duration.

In Eq. (1), both ΔP and T are functions of depth. The creep rates in salt vary with temperature. However, from casing shoe to open-hole bottom, the difference between uppermost (at hole bottom) and lowermost (at casing shoe) temperatures is less than 5 °C; hence, a uniform creep coefficient, C_{creep}, is used for the open hole. Influence of the pressure gap, ΔP, is more significant, and the rate of volume change due to creep closure is integrated along the open hole — see Eq. (2). The exponent n is 3.1 for Étrez salt (Brouard and Bérest, 1998):

$$\dot{V}_{creep} = -C_{creep} S_{ann} \int_{H_{cas}}^{H} \left[-P_{tub}^{wh} + (\gamma_R - \gamma_b) z\right]^n dz \tag{2}$$

7.2 Permeation in the wellbore

The characteristic time for transient permeation in salt can be a few weeks to few months. Hence, transient flow evolution and the pressure history of the wellbore must be taken into account [Eq. (3)]. The relevant parameters are: open-hole height, h = 352 m (1154 ft); porosity of the lower salt formation, ϕ = 0.01 (Durup, 1994); open-hole radius, r_w ; and the total compressibility taken to be c_t = 6 x 10^{-5} bar^{-1} (4 x 10^{-6}/psi). The possible near-wellbore damage created in the salt layers during drilling is neglected. The non-dimensional flow rate, Q_D, for constant wellbore pressure is computed from the Laplace transformation of unsteady-state Darcy's equation (Van Everdingen and Hurst, 1949), resulting in

$$Q_{perm} = \int_0^t \frac{2\pi kh}{\mu} \dot{P}_{tub}^{wh}(\tau) \times Q_D \left(\frac{k[t-\tau]}{\mu\phi c_t r_w^2}\right) \mathrm{d}\tau \qquad (3)$$

Note that this solution holds for an infinitely long cylinder. For such a geometry, no steady-state regime can be reached even after an infinite period of time. The actual open hole is an elongated cylinder [diameter $14^{3/4"}$, length 352 m (or 1154 ft); it is not infinite. However, the difference between the two geometries is not relevant except when very long periods of time are considered.

7.3 Mass conservation in wellbore

It can be inferred from Fig. 3 that the variations of brine density resulting from temperature distribution in the well is less than 2%. Hence, brine density in the well is assumed to be uniform. The mass balance for fluids in the well is given by Eq. (4). It is assumed that salt is impermeable to diesel. The total well compressibility, (βV), has a value of 3.8 L/bar during Phase 1. The injection rate at the wellhead, Q_{tub}^{wh}, was zero during this phase. Between April 22 and April 29, (Phase 2), the average injection rate at the wellhead, $\dot{P}_{tub}^{wh}$, was almost zero:

$$(\beta V)\dot{P}_{tub}^{wh}(t) = Q_{tub}^{wh}(t) + C_{creep} S_{ann} \int_{H_{cas}}^{H} \left[-P_{tub}^{wh} + (\gamma_R - \gamma_b)z\right]^n dz - \int_0^t \frac{2\pi kh}{\mu} \dot{P}_{tub}^{wh}(\tau) \times Q_D \left(\frac{k[t-\tau]}{\mu\phi c_t r_w^2}\right) \mathrm{d}\tau \qquad (4)$$

7.4 Solving the minimization problem

Using the simplifications made above, only two unknown quantities appear in Eq. (4), C_{creep} (/MPa^n/yr) and k/μ (m^2/cP), which are relative to the creep rate and the formation mobility, respectively. Their values can be estimated by minimizing the error R^2, which quantifies the average variation between the simulated data and the test data [Eq. (4)]:

$$min_{C_{creep},k/\mu}\left\{R^2 = \sum\left[P^{wh}_{tub,test} - P^{wh}_{tub,simul}(C_{creep},\frac{k}{\mu})\right]^2\right\} \quad (5)$$

$$C_{creep} \in [0.5, 50] \times 10^{-6}\ \frac{1}{\mathrm{MPa^n yr}}$$

$$\frac{k}{\mu} = [0.1, 100] \times\ 10^{-21}\ \mathrm{m^2/cP}$$

Data from Phase 1 are sufficient to estimate the creep coefficient and the average mobility of the wellbore (including open hole, casing shoe and steel casing). Data from Phase 2 enable the estimation of salt permeability by isolating the leak through the casing shoe and cementing. The simulations are performed using Eq. (4) for the time periods highlighted by the double-headed arrows in Fig. 5. The pressure history from the test is used to start the simulation, and the simulated pressures are used for the subsequent timesteps. Equation (4) is nonlinear, and a 4th-order Runge-Kutta scheme is used to solve it. The steady-state creep coefficient for the Étrez lower layer is A^* = 3 x 10^{-6} /MPa^n/yr (Brouard and Bérest, 1998); the pseudo steady-state creep coefficient at early times, C_{creep}, is expected to be slightly larger than A^*. The permeability of the lower salt layer is k = 4.6-19 x 10^{-21} m^2 [Brouard et al., 2001]. The solution space in Eq. (5) is chosen to investigate one order of magnitude on either side of Étrez values. Brine viscosity at 60 °C is μ = 9 x 10^{-4} Pa.s (Fig. 3).

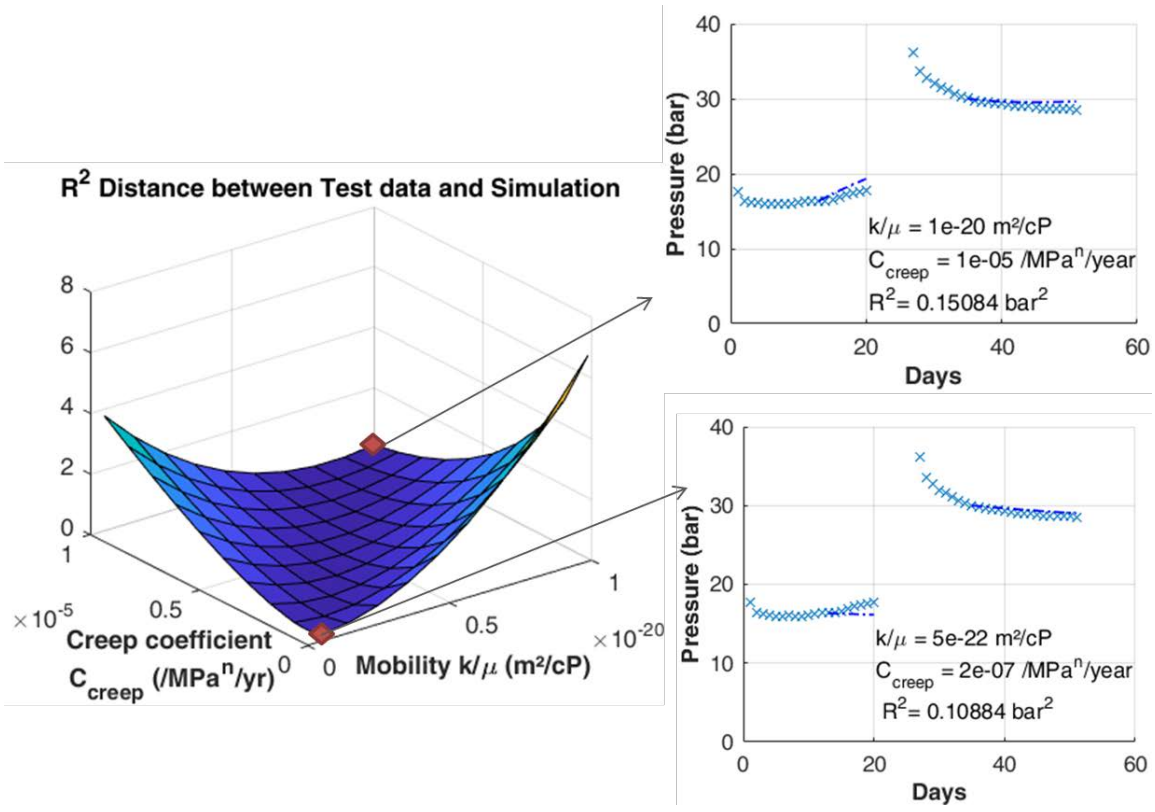

Figure 8: Error R² at boundary points. [Comparison of Test data ('x') and simulation (dotted lines) does not show a good match.]

The solution space is reduced after an initial iteration and the error for the reduced solution space is evaluated in Fig. 8. R^2 is the 'distance' between the test data and the simulated data for different combinations of mobility and creep coefficients. The error is minimum along one of the diagonals and maximum along the other. The two boundary points highlighted in Fig. 8 do not provide a good match against the test data. However, there are interior points with smaller error values (Fig. 9). The solution space is reduced further to the neighborhood of these points and discretized on a finer scale. Figure 10 shows the best solution which corresponds to a permeability of $k = 6 \times 10^{-21}$ m^2 (6 nD).

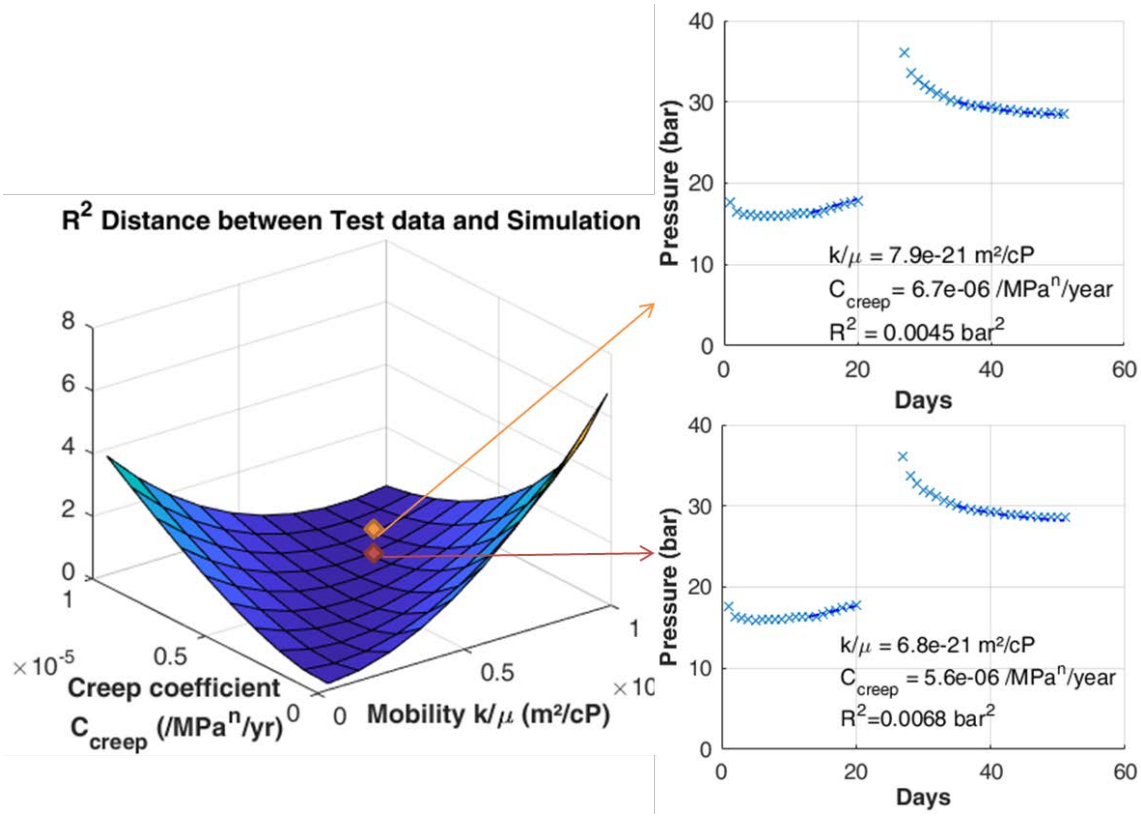

Figure 9: Error R^2 at interior points are much lower than that at boundary points. [Comparison of test data ('x') and simulation (dotted lines) shows reasonable agreement.]

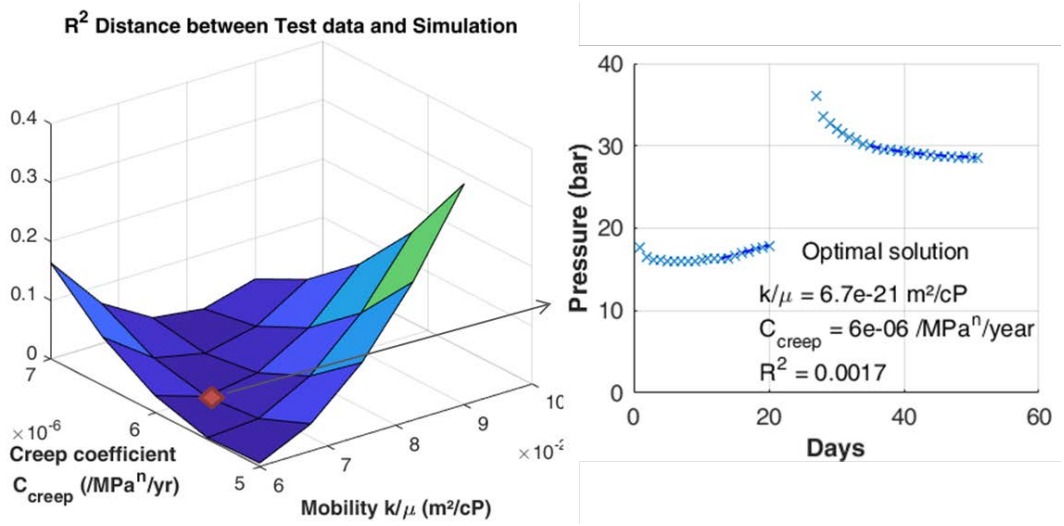

Figure 10: Error R^2 reduces further upon finer discretization. (There is very good agreement between the Test data ('x') and simulation (dotted lines) —— the optimal solution. Error R^2 here is the least amongst all crossplots.

Small leaks through the casing shoe and cementing are common. At the beginning of Phase 2, the casing shoe was covered with diesel, whose leak rate is negligible when compared to that of brine. This allowed the salt formation to be tested in isolation and the salt permeability estimated (Fig. 11). The creep coefficient from the earlier estimation is used. The average permeability of the open hole is estimated to be $k = 4 \times 10^{-21}$ m^2, slightly less than the average permeability of the wellbore. The estimated salt permeability is slightly less than the estimations by Brouard et al. (2001) [shown on Table 3]. This is expected because the estimations by Brouard et al. [2001] also include the seepage through casing shoe. (During the tests described by Brouard et al., the steel casing seepage was isolated by a packer assembly.) In addition, the creep coefficient compares well against the estimates for the lower salt layer at Étrez (Table 3). (A^* is the steady-state creep coefficient, whereas C_{creep} is a pseudo steady-state coefficient).

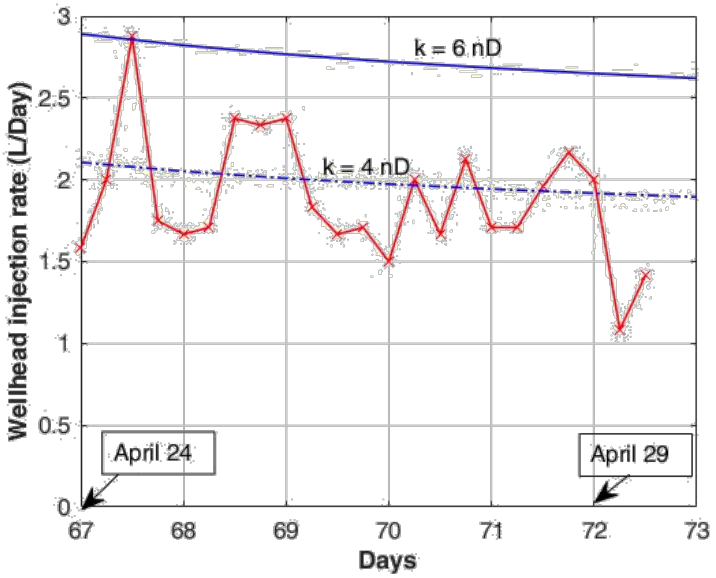

Figure 11: Average open-hole permeability estimated from Phase 2 data (red curve) compared to wellbore average permeability (blue curve).

Table 4: Comparison of test results with those of the lower salt layer at Étrez.

Quantity	AT032 Marboz	Étrez
Creep coefficient	C_{creep} = 6 10^{-6} /MPa^n/yr	A^* = 3 10^{-6} /MPa^n/yr
Salt permeability	k_{salt} = 4 10^{-21} m^2	$k_{salt+cas\text{-}shoe}$ = 4.6-19 x 10^{-21} m^2
Well permeability	k_{well} = 6 10^{-21} m^2	

Conclusions

The coefficients describing average well permeability, open-hole permeability and closure rate of AT032, a borehole drilled at Marboz, France, were estimated. The assessed creep coefficient and permeabilities are in good agreement with those measured at Étrez in the same salt formation at a 6-mile distance from Marboz. This well is found to be quite tight, with leak rates less than 1 L/day (2 bbls/year).

A new method (*discrete WTLog*) had been designed to measure salt permeability as a function of depth. However, the resolution of this method was not good enough to provide useful results, as average salt permeability (4 x 10^{-21} m^2, or 4 nD) is too small. Longer testing periods and more accurate pressure sensors might provide better results.

Acknowledgements

The work presented here was conducted within the framework of a Ph.D. thesis funded by TOTAL SA. The authors would like to thank the INOVYN staff for their valuable assistance with the in-situ tests.

References

Bérest P., Brouard B., Karimi-Jafari M., Van Sambeek L. (2007). *Transient behavior of salt caverns. Interpretation of Mechanical Integrity Tests*. Int. J. Rock Mech. Min. Sc. (44) 767-786.

Brouard B., Bérest P. (1998). *A tentative classification of salts according to their creep properties.* Proc. SMRI Spring Meeting, New Orleans, Louisiana, 18-38.

Brouard B., Bérest P., Durup J.G. (2001). *In-situ salt permeability testing.* Proc. SMRI Fall Meeting, Albuquerque, New Mexico, 139-157.

Brouard B., Bérest P., de Greef V., Beraud J.F., Lheur C., Hertz E. (2013). *Creep closure rate of a shallow salt cavern at Gellenoncour*t, *France*. Int. J. Rock Mech. Min. Sc. (62), 42-50.

Curial A. (1986). *La sédimentation salifère et suprasalifère du Palogène Bressan*. PhD. thesis, Université Claude Bernard Lyon I, October 1986.

Durup JG. (1994). *Long term tests for tightness evaluations with brine and gas in salt.* Proc. SMRI Fall Meeting, Hannover, Germany, 1994.

Lampe B., Ratigan J.L. (2014). *Pitfalls of a Nitrogen-Brine interface Mechanical Integrity Test*. Proc. SMRI Spring Meeting, San Antonio, Texas, 19-30.

Manivannan S., Bérest P., Brouard B. (2015). *Effects of changes in the pressure and temperature of the testing fluid during a liquid-liquid MIT*. Proc. SMRI Fall Meeting, Santander, Spain, 3-19.

Manivannan S., Bérest P. (2018). *Closure of a cylindrical hole in a Norton-Hoff medium.* Submitted for publication in Rock Mechanics and Rock Engineering.

Manivannan. S., Jacques A., Brouard B., Bérest. P. (2017). *A Novel Injectivity and Permeability Log for Tight Reservoirs*. SPE Europec featured at 79th EAGE Conference and Exhibition, Paris, France, 12–15 June. SPE-185860-MS. https://doi.org/10.2118/185860-MS.

Skaug NT., Ratigan JL., Lampe BC. (2011). *A critical look at the Nitrogen/Brine Interface Mechanical Integrity Test*. Proc. SMRI Fall Meeting, York, UK, 324-332.

Van Everdingen, AF., Hurst, W. (1949). *The application of the Laplace transformation to flow problems in reservoirs*. Trans. AIME 186, 305-324.